Equivalent Shear Force Method for Detecting the Speed and Axles of Moving Vehicles on Bridges

Lu Deng, Ph.D., M.ASCE[1]; Wei He[2]; Yang Yu[3]; and C. S. Cai, Ph.D., F.ASCE[4]

Abstract: Traffic monitoring, particularly on the gross vehicle weight (GVW) and axle weights (AWs) of heavy trucks, provides valuable information for the design and performance evaluation of bridges. Bridge weigh-in-motion (BWIM) is a recently developed technology that uses the bridge as a scale to estimate vehicle weights. For BWIM systems, the acquisition of vehicle speed and axle spacing (AS) is a prerequisite for accurate identification of the AWs and GVW. Traditionally, axle detectors are placed on the road surface to detect vehicle axles. However, axle detectors are not durable due to their exposure to the traffic. Also, their installation and maintenance also cause disruption to the traffic. For these reasons, the concept of the nothing-on-road (NOR) BWIM is proposed. Most existing NOR BWIM systems require additional sensors for axle detection, which limits their applicability. In this paper, a novel equivalent shear force method (ESF) is proposed to identify vehicle speed and AS by using the flexural strain signal acquired from the weighting sensors. Compared with the existing NOR BWIM systems, the proposed method does not require additional sensors for axle detection, making it desirable for commercial BWIM systems. The effectiveness and accuracy of the proposed method are demonstrated through numerical simulations and validated through an experiment using scaled model tests. Parametric studies are also conducted to investigate the effects of various factors on the accuracy of the proposed method. **DOI: 10.1061/(ASCE)BE.1943-5592.0001278.**

Author keywords: Equivalent shear force method (ESF); Bridge weigh-in-motion (BWIM); Strain; Axle spacing (AS); Vehicle weight; Structural health monitoring.

Introduction

Bridge weigh-in-motion (BWIM) offers an efficient way to obtain the weight information of passing vehicles using an instrumented bridge (Moses 1979; Zolghadri et al. 2016). This information is valuable for the management of transportation networks and safety assessment of bridges (Lydon et al. 2016; Jacob and O'Brien 2005). Extensive research has been devoted to developing new BWIM algorithms and improving the identification accuracy of BWIM systems in the last several decades (Peters 1984; Jacob and O'Brien 1998; Laboratoire Central des Ponts et Chaussées 2001; O'Brien et al. 2009; Žnidarič et al. 2015). A comprehensive state-of-the-art review of existing BWIM algorithms and systems was presented by Yu et al. (2016). Lydon et al. (2016) also reviewed recent achievement of BWIM systems and highlighted the applications of BWIM data.

To identify the axle weights (AWs) and gross weight of vehicles, accurate axle detection is required by most BWIM systems. Typically, a BWIM system includes weighing sensors and axle detecting devices (Moses 1979). Axle detection can use pavement-based sensors, such as tape switches, pneumatic tubes, and piezoceramic sensors. Although pavement-based sensors can usually achieve accurate detection, they are not ideal for BWIM applications because they are not durable and can cause disruption to the traffic (Laboratoire Central des Ponts et Chaussées 2001; Chatterjee et al. 2006; Zhao et al. 2014). With the goal of freeing the use of axle detectors on the road surface, the concept of nothing-on-road (NOR) systems and the free-of-axle detector (FAD) algorithms were introduced in the Weighing-in-Motion of Axles and Vehicles for Europe (WAVE) project (Laboratoire Central des Ponts et Chaussées 2001). The FAD methods use additional FAD sensors installed on the soffit of the bridge to measure the local bridge responses, which contain the information of vehicle axles. However, the FAD methods are not suitable for certain types of bridges and are susceptible to wheel transverse positions (O'Brien et al. 2012; Ieng et al. 2012; Kalin et al. 2006). To overcome these disadvantages, several alternative axle detection strategies have been developed for the NOR BWIM systems. O'Brien et al. (2012) and Bao et al. (2016) proposed measuring the shear strain to identify vehicle axles. Kalhori et al. (2017) found that using the shear strain measured at the support of the bridge can provide more accurate axle detection than those measured at midspan and quarter span. Nevertheless, the direct measurement of shear strain is not easy in practice and would require shear strain sensors in addition to the strain sensors in the BWIM system. Lydon et al. (2017) developed a NOR BWIM system based on advanced fiber optical sensors. Ojio et al. (2016) proposed a contactless BWIM system using roadside vision systems to monitor and identify vehicle speed and axle spacing (AS). Yu et al. (2017a) proposed a NOR BWIM method that can identify the vehicle's transverse position using only the weighing sensors. In addition, wavelet analysis, as a powerful pattern recognition technique, has also been applied to facilitate axle detection by some researchers (Chatterjee et al. 2006; Yu et al. 2017b; Dunne

[1]Professor, Key Laboratory for Wind and Bridge Engineering of Hunan Province, Hunan Univ., Changsha, Hunan 410082, China (corresponding author). Email: denglu@hnu.edu.cn

[2]Research Assistant, College of Civil Engineering, Hunan Univ., Changsha, Hunan 410082, China. Email: hewei.hnu@gmail.com

[3]Research Assistant, Dept. of Civil and Environmental Engineering, Louisiana State Univ., Baton Rouge, LA 70803. Email: josephyangyu@gmail.com

[4]Professor, Dept. of Civil and Environmental Engineering, Louisiana State Univ., Baton Rouge, LA 70803. Email: cscai@lsu.edu

Note. This manuscript was submitted on August 28, 2017; approved on March 28, 2018; published online on June 13, 2018. Discussion period open until November 13, 2018; separate discussions must be submitted for individual papers. This paper is part of the ***Journal of Bridge Engineering***, © ASCE, ISSN 1084-0702.

et al. 2005; Lechner et al. 2010). Nevertheless, this technique is susceptible to the errors in the original data (Lydon et al. 2016).

For bending moment-based BWIM systems, it is desirable to directly extract axle information from the global strain signals. Wall et al. (2009) calculated the second derivative of the time history of bridge global bending response with respect to time for the identification of vehicle speed and AS. Kalhori et al. (2017) identified vehicle axles using the peak-to-peak approach, which uses flexural strains, although some axles might be missed under some circumstances. Yu et al. (2017b) applied the wavelet transformation of the bridge global response to achieve the axle detection using only the weighing sensor. However, these methods use delicate features of the flexural response and are generally susceptible to measurement noises and dynamic effects due to the vibration of the vehicle–bridge system.

In this study, a novel equivalent shear force (ESF) method was proposed to estimate vehicle speed and AS. This method directly uses the flexural strain signals acquired from weighing sensors to detect the vehicle axles. To demonstrate the effectiveness and accuracy of the proposed ESF method, extensive numerical simulations based on a three-dimensional (3D) bridge-vehicle interaction (BVI) system and scale model tests are conducted. The effects of various factors on the accuracy of the proposed method also are investigated.

Methodology for Detecting Vehicle Speed and Axles

ESF Method

Fig. 1(a) shows a linear-elastic beam AB with arbitrary support conditions. P, Q, and O are three consecutive points on beam AB, whereas Point O is located at the middle of Points P and Q. Also, l_A, l, and l_B are the length of segments AP, PQ, and QB, respectively. The reaction forces of the beam AB are represented by M_A, M_B, F_A, and F_B, which are functions of x, as shown in Fig. 1(a).

When the beam AB is subjected to a concentrated force F applied at a distance of x from Point A, the bending moment at Positions P and Q of the beam AB can be expressed as

$$M_P = \begin{cases} M_A(x)+F_A(x)l_A-F(l_A-x) & 0\le x<l_A \\ M_A(x)+F_A(x)l_A & l_A\le x<l_A+l+l_B \end{cases}$$

$$M_Q = \begin{cases} M_A(x)+F_A(x)(l_A+l)-F(l_A+l-x) & 0\le x<l_A+l \\ M_A(x)+F_A(x)(l_A+l) & l_A+l\le x<l_A+l+l_B \end{cases} \tag{1}$$

From Eq. (1), the following two variables can be defined and derived:

$$V^{\mathrm{E}}(x) \triangleq \frac{M_Q-M_P}{l} = G(x)+F_A(x)$$

$$\text{where } G(x) = \begin{cases} -F & 0\le x<l_A \\ -F\left(1-\dfrac{x}{l}\right) & l_A\le x<l_A+l \\ 0 & l_A+l\le x\le l_A+l+l_B \end{cases} \tag{2}$$

For the purpose of illustration, the influence lines for $F_A(x)$, $G(x)$, and $V^E(x)$ for a beam with a fixed support on the left end and a roller support on the right end are obtained based on Eq. (2) by assuming F = 1, and the results are plotted in Fig. 1(b). The figures

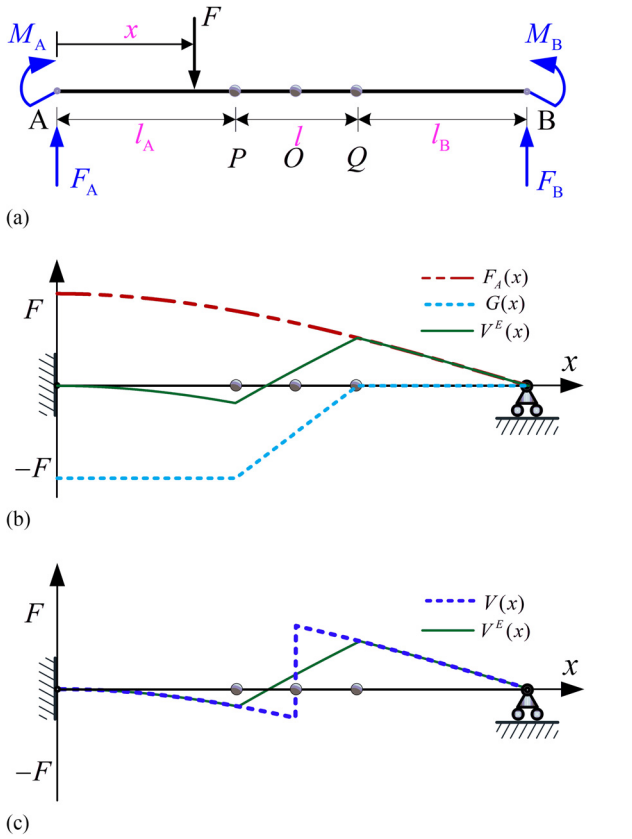

Fig. 1. ESF method: (a) Beam AB with arbitrary boundary conditions; (b) the influence lines of $F_A(x)$, $G(x)$, and $V^E(x)$; and (c) the influence line for the shear force at Point O and the ESF of segment PQ.

shows that $V^E(x)$ has two sudden changes of slope corresponding to a valley and a peak on its influence line.

In fact, when the distance l of PQ approaches zero, based on the theory of mechanics of materials, V^E, which is derived by the moments at Points P and Q as shown in Eq. (2), is the shear force of the center point of PQ ($V = \mathrm{d}M/\mathrm{d}x = \lim_{l\to 0} V^E$). Therefore, V^E is called the ESF of PQ hereafter. The influence line of the shear force V at Point O and the influence line of the ESF of PQ are plotted in Fig. 1(c). When Points P and Q approach Point O, the ESF curve shown in Fig. 1(c) will converge to the shear force at Point O.

Axle Detection

The sudden changes of the slope of V^E can be used to identify axle passing. First, two segments P_1Q_1 and P_2Q_2 were selected, as shown in Fig. 2(a). The lengths of the two segments are denoted as l_1 and l_2, respectively. The distance between the centers of the two segments is L, as shown in Fig. 2(a). Then, the ESF of the two segments can be obtained using Eq. (2). Based on the characteristic of the ESF, if an N-axle vehicle passes the bridge, there will be N groups of valleys and peaks on the ESF of a segment. Thus, the axles can be identified as the number of valleys or peaks on the ESF curve. The vehicle speed can be predicted using the time lag between the ESFs of the two segments and the known distance L. It should be noted that, theoretically, the vehicle speed can be identified using the time lag between the valley and the peak. However, in reality, the dynamic effect and measurement noises tend to shift the peaks and valleys away from their theoretical locations, making it difficult to accurately identify the vehicle speed using only one

segment. Therefore, two segments with a center spacing of L were used for identification.

Figs. 2(b and c) show the static bending moment and the ESF of two segments of a simply supported Beam AB subjected to two moving loads with a spacing of d. The x-axis represents the location of the first axle, and the y-axis represents the bending moments or the ESF. From Fig. 2, the number of axles can be identified by counting the number of valleys (t_{11}^1 and t_{21}^1 relative to P_1 on V_1^E, or t_{11}^2 and t_{21}^2 relative to P_2 on V_2^E) or peaks (t_{12}^1 and t_{22}^1 relative to Q_1 on V_1^E, or t_{12}^2 and t_{22}^2 relative to Q_2 on V_2^E). Then, the vehicle speed can be predicted as

$$v = \frac{L}{\Delta T} = \frac{L}{\frac{t_{11}^2 + t_{12}^2}{2} - \frac{t_{11}^1 + t_{12}^1}{2}} \text{ or } v = \frac{L}{\frac{t_{21}^2 + t_{22}^2}{2} - \frac{t_{21}^1 + t_{22}^1}{2}} \tag{3}$$

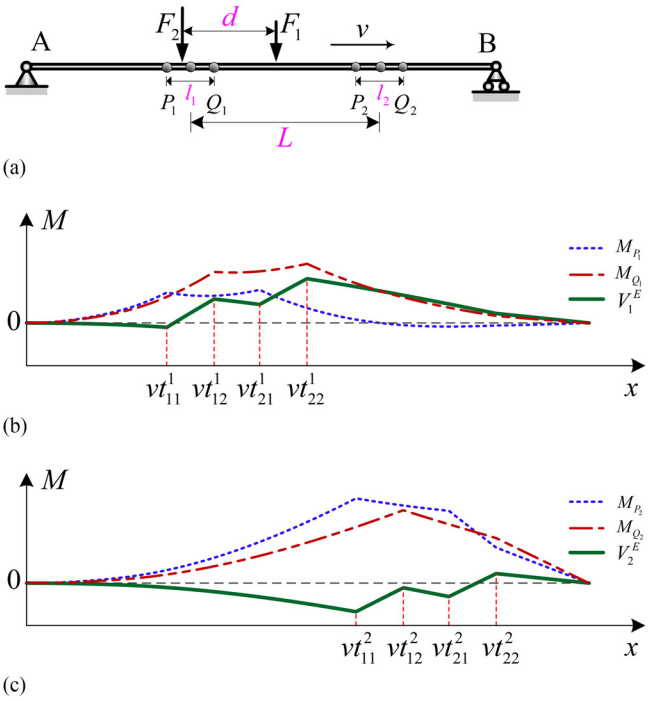

Fig. 2. Bending moment and ESFs of a beam under two moving loads: (a) a simply supported beam AB subject to two moving loads; (b) the static moments at P_1 and Q_1, and ESF of P_1Q_1 (V_1^E); and (c) the static moments at P_2 and Q_2, and ESF of P_2Q_2 (V_2^E).

where ΔT = time lag between V_1^E and V_2^E. It can also be automatically determined by using an alternatively cross-correlation algorithm proposed by Kalin et al. (2006). After the vehicle speed is obtained, the AS can be easily calculated as

$$d = v\left(\frac{t_{21}^1 + t_{22}^1}{2} - \frac{t_{11}^1 + t_{12}^1}{2}\right) \text{ or } d = v\left(\frac{t_{21}^2 + t_{22}^2}{2} - \frac{t_{11}^2 + t_{12}^2}{2}\right) \tag{4}$$

Based on the previous discussion, it can be seen that two groups of measurement points, with two points in each group, are needed to identify the vehicle speed and AS. Nevertheless, in practice, only three measurement points are needed because the two segments can share one measurement point located in the middle. In addition, it should be mentioned that the ESF method can only be used to identify axles whose spacing is larger than the spacing of the two adjacent measurement points. For those closely spaced axles (for example, an axle group), the proposed method may automatically treat them as one single axle in the identification process, as will be demonstrated in the numerical simulations and model tests.

In-service bridges under routine traffic loads can normally be considered as linear-elastic systems; namely, the global bending moment is linearly related to the flexural strain. Taking a multigirder bridge, for example, the total global bending moment of the

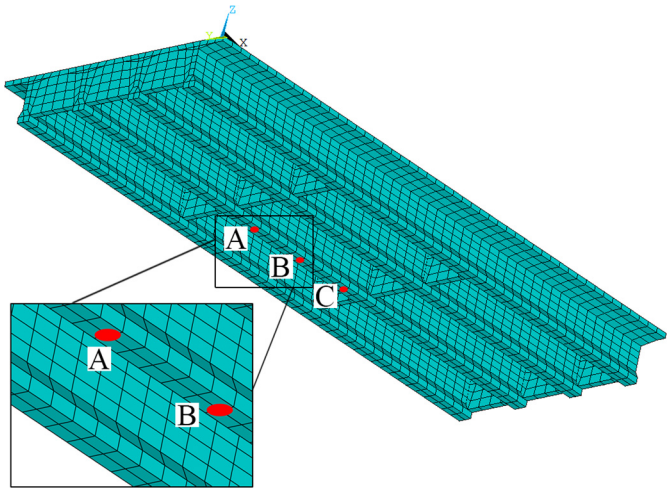

Fig. 4. Finite-element model of the bridge and locations of the measurement stations.

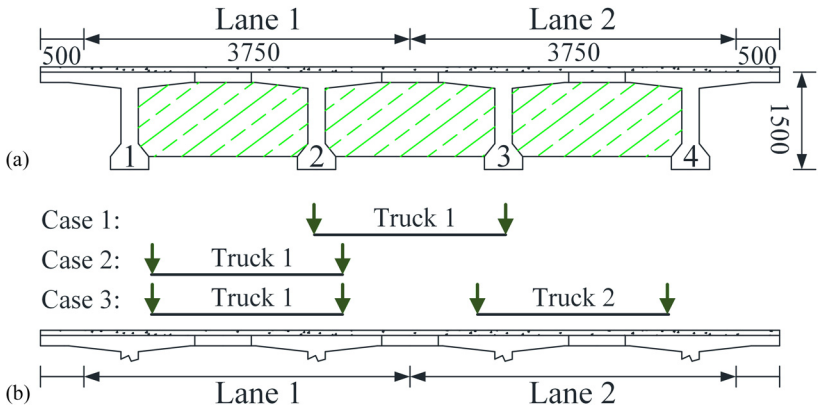

Fig. 3. (a) Bridge cross section (unit: millimeters); and (b) considered loading cases.

bridge at a cross section can be calculated based on the recorded normal strain as follows:

$$M_s = \sum_{i=1}^{n} EW_i \varepsilon_{s,i}, \quad s = \{P_1, Q_1, P_2, Q_2\} \tag{5}$$

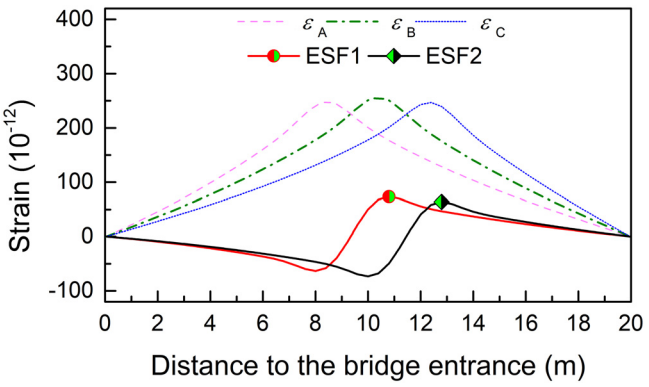

Fig. 5. Influence lines for the longitudinal strains of measurement stations and ESFs of AB and BC under Loading Case 1.

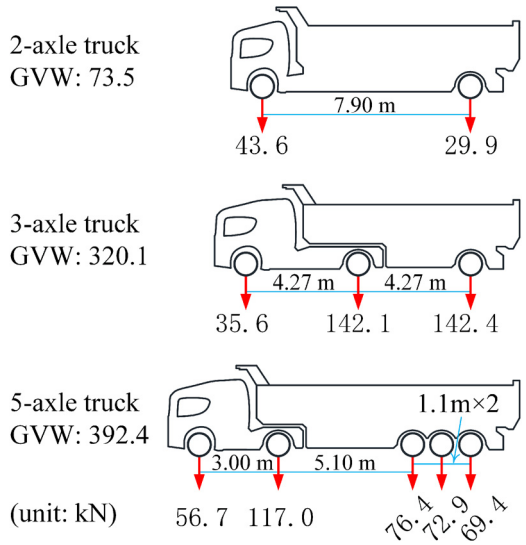

Fig. 6. AW distribution of the three trucks. GWV = gross vehicle weight.

where E = modulus of elasticity of the bridge material; W_i = section modulus of the ith girder; and $\varepsilon_{s,i}$ = normal strain of the ith girder at section s. However, it was found in this study that using the strain information from all girders is not necessary because the strain from one particular girder that bears a significant portion of vehicle loads can fulfill the requirement of identifying the vehicle speed and AS, even under different transverse locations of the moving vehicle. Therefore, there is no need to install sensors on all girders in the lateral direction, and the strain information from the girder that bears the largest amount of vehicle loads was selected in the present study, namely

$$\mathrm{ESF}_j = V_j^E = \frac{M_{Q_j} - M_{P_j}}{l_j} = \frac{EW}{l_j}(\varepsilon_{Q_j} - \varepsilon_{P_j}) \tag{6}$$

For the sake of convenience, EW/l_j is omitted in the following analysis because it is a constant scalar.

Table 1. Parameters considered in the numerical simulation

Parameter	Values
Vehicle speed (m/s)	10, 15, 20, 25, 30
RSC	Smooth, very good, good, average
Truck type	2-axle truck, 3-axle truck, 5-axle truck
Loading cases	1: one truck along the centerline of the bridge
	2: one truck along the centerline of Lane 1
	3: two trucks in both traffic lanes

Note: RSC = road surface condition.

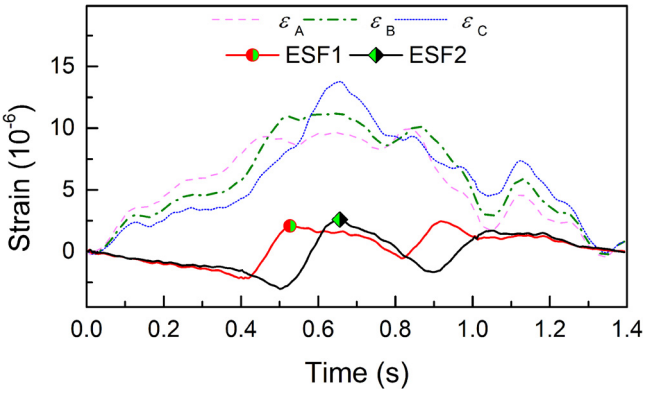

Fig. 8. Typical simulated bending strains and derived ESFs (Loading Case 1, 2-axle truck, v = 20 m/s, average RSC).

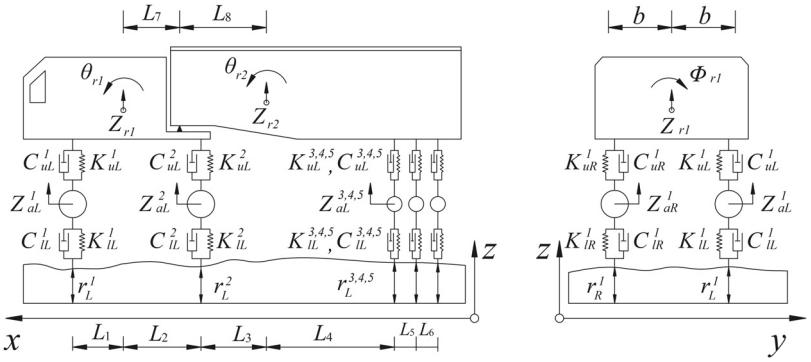

Fig. 7. Analytical model of the 5-axle truck.

Numerical Simulations

Bridge-Vehicle Coupled System

Dynamic Equation of Bridge and Vehicle

The dynamic equations of motion of bridge and vehicle can be expressed as follows:

$$\mathbf{M}_b\ddot{d}_b + \mathbf{C}_b\dot{d}_b + \mathbf{K}_b d_b = \mathbf{F}_b$$

$$\mathbf{M}_v\ddot{d}_v + \mathbf{C}_v\dot{d}_v + \mathbf{K}_v d_v = \mathbf{F}_v \tag{7}$$

where $\mathbf{M}_b$, $\mathbf{M}_v$, $\mathbf{C}_b$, $\mathbf{C}_v$, $\mathbf{K}_b$, and $\mathbf{K}_v$ = mass, damping, and stiffness matrices of the bridge and the vehicle, respectively; d_b and d_v are the displacement vectors (in the vertical direction) of the bridge and the vehicle, respectively; and $\mathbf{F}_b$ and $\mathbf{F}_v$ are the vectors containing all the external forces acting on the bridge and the vehicle, respectively. In a vehicle-bridge system, the deformation of the vehicle spring ΔL, which determines the interaction forces at the contact points, can be expressed as a function of the vertical displacement of the vehicle body d_v, the bridge deflection at the contact point d_{b_contact}, and the road surface profile $r(x)$, which will be introduced in the following section:

$$\Delta L = d_v - d_{b\_\text{contact}} - r(x) \tag{8}$$

By using the force and displacement compatibility at the contacting points between the bridge and the vehicle, the motion

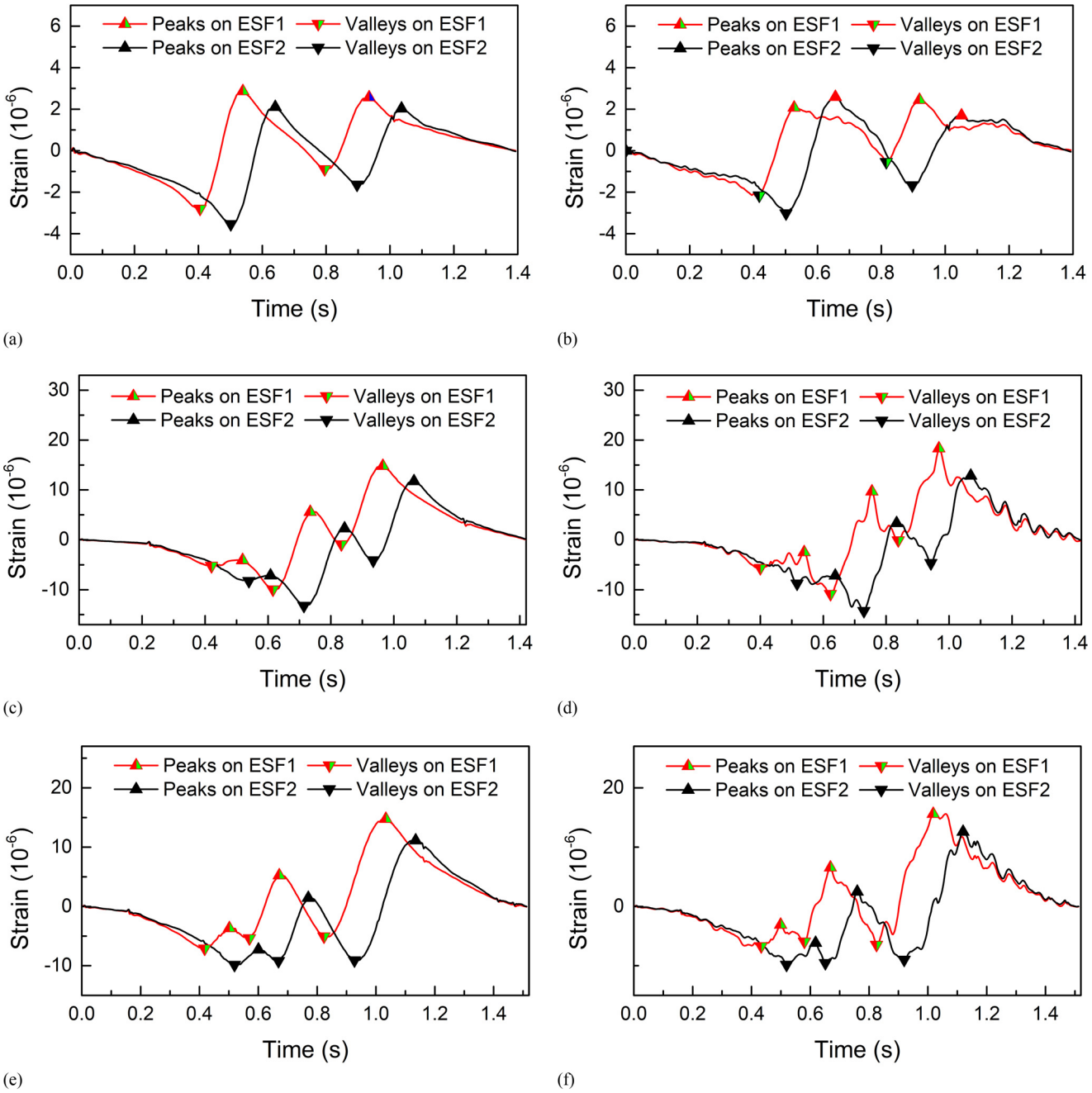

Fig. 9. Simulated ESFs under different loading scenarios (Loading Case 1, $v = 20$ m/s): (a) 2-axle truck, smooth RSC; (b) 2-axle truck, average RSC; (c) 3-axle truck, smooth RSC; (d) 3-axle truck, average RSC; (e) 5-axle truck, smooth RSC; and (f) 5-axle truck, average RSC.

equations of the bridge and the vehicle can be coupled as follows:

$$\begin{bmatrix} \mathbf{M}_b & \\ & \mathbf{M}_v \end{bmatrix} \begin{Bmatrix} \ddot{d}_b \\ \ddot{d}_v \end{Bmatrix} + \begin{bmatrix} \mathbf{C}_b & \mathbf{C}_{bv} \\ \mathbf{C}_{vb} & \mathbf{C}_v \end{bmatrix} \begin{Bmatrix} \dot{d}_b \\ \dot{d}_v \end{Bmatrix} + \begin{bmatrix} \mathbf{K}_b & \mathbf{K}_{bv} \\ \mathbf{K}_{vb} & \mathbf{K}_v \end{bmatrix} \begin{Bmatrix} d_b \\ d_v \end{Bmatrix} = \begin{Bmatrix} \mathbf{F}_{br} \\ \mathbf{F}_{vr} + \mathbf{F}_{vg} \end{Bmatrix} \tag{9}$$

where $\mathbf{C}_{bv}$, $\mathbf{C}_{vb}$, $\mathbf{K}_{bv}$, and $\mathbf{K}_{vb}$ are time-dependent terms related to the tire-road contact forces; $\mathbf{F}_{bv}$ and $\mathbf{F}_{vb}$ are the equivalent nodal forces of the wheel-road contact forces acting on the bridge and the vehicle, respectively; and $\mathbf{F}_{vg}$ is the gravity force vector of the vehicle. The details of deriving these equations can be found in Deng and Cai (2010a, b) and are not introduced here for the sake of brevity.

Road Surface Condition

Road surface roughness is a main source of excitation for the vibration of the bridge-vehicle system. It can be described by a zero-mean stationary Gaussian stochastic process, which can be generated through Eq. (10) (Dodds and Robson 1973)

$$r(x) = \sum_{k=1}^{N} \sqrt{2\varphi(n_k)\Delta n} \cos(2\pi n_k x + \theta_k)$$

$$\varphi(n) = \varphi(n_0)\left(\frac{n}{n_0}\right)^{-2} (n_1 < n < n_2) \tag{10}$$

where $\varphi()$ = power spectrum density function for the road surface elevation (cubic meter per cycle); $\varphi(n_0)$ is the roughness coefficient (cubic meter per cycle); n = spatial frequency (cycle per meter); n_0 = discontinuity frequency of 0.5π cycle/m; n_1 and n_2 = lower and upper cut-off frequencies, respectively; θ_k = random phase angle that follows a uniform distribution from 0 to 2π; and n_k = wave number (cycle per meter). The ISO (1995) classified the road surface condition (RSC) based on different roughness coefficients. Based on the ISO classification, a total of four different RSCs, namely, smooth, very good, good, and average, were considered in the present study, with corresponding roughness coefficients of 0, 5×10^{-6}, 20×10^{-6}, and 80×10^{-6} m^3/cycle, respectively.

Solving the BVI Problem

Eq. (10) can be solved using numerical integration algorithms. A MATLAB program was developed to solve the BVI problem using the Newmark-β method in the time domain. The BVI model has also been validated using field measurements by Cai et al. (2007) and Deng and Cai (2011). The strain of the bridge can be calculated based on the bridge dynamic displacement responses by

$$\varepsilon = B \cdot d_b \tag{11}$$

where B is the strain-displacement relationship matrix assembled with the derivatives of the element shape functions with respect to x, y, and z, and can be derived following a standard finite-element formulation process.

Case Description

Bridge Model

In the present study, a multigirder bridge with four identical T-beams was used in the numerical simulations. The bridge's cross section and the selected loading positions are plotted in Fig. 3. The bridge was modeled using solid elements in ANSYS. The finite-element model of the bridge is shown in Fig. 4. In the simulation study, three measurement stations with an equal spacing of 2 m are selected on the soffit of Girder 2, which bears the largest proportion of vehicle loads. As shown in Fig. 4, the three measurement stations are denoted by A, B, and C in which Station B is located at the midspan.

Table 2. RMS of the relative identification errors (%) of the three trucks (Loading Case 1)

		RMS of identification error (%)							
		2-axle truck		3-axle truck			5-axle truck		
RSC	True speed (m/s)	Speed	AS	Speed	AS_1	AS_2	Speed	AS_1	AS_2
Smooth	10	0.31	0.16	0.41	0.23	0.36	0.21	2.29	2.38
	15	0.78	0.38	0.31	3.15	0.50	0.93	2.79	1.54
	20	0.68	0.01	0.47	1.04	1.03	0.68	2.73	1.81
	25	1.30	0.63	0.68	3.47	1.11	0.16	1.06	1.64
	30	2.22	0.77	0.05	1.46	2.64	0.37	2.97	0.62
Very good	10	1.62	1.63	1.66	2.52	2.57	1.06	1.89	1.21
	15	0.70	0.90	1.35	3.17	2.18	2.06	2.09	1.69
	20	1.34	0.87	1.42	3.39	1.90	1.75	2.00	2.01
	25	0.51	0.89	2.11	3.63	4.00	1.12	1.29	1.43
	30	1.82	0.82	1.50	3.54	2.78	1.23	2.82	1.41
Good	10	1.25	1.03	1.92	4.29	3.68	1.32	2.03	0.84
	15	0.48	1.23	1.53	2.87	3.52	1.28	2.04	1.60
	20	1.07	0.89	1.80	2.68	3.38	1.56	1.73	2.85
	25	1.24	1.13	2.10	4.41	3.87	1.58	2.43	2.97
	30	1.40	1.51	2.51	3.00	3.08	1.10	2.52	2.46
Average	10	1.03	2.03	2.70	3.25	2.37	1.12	2.49	2.26
	15	1.39	2.22	1.84	2.59	3.02	2.41	1.70	2.98
	20	2.49	3.03	2.26	3.13	3.86	1.42	3.03	2.44
	25	1.83	1.63	2.38	2.95	2.89	1.99	4.05	2.56
	30	1.52	2.03	1.79	3.13	2.74	1.80	2.94	3.68

Note: RSC = road surface condition.

The ESFs of AB and BC were calculated using the longitudinal strains collected from the measurement stations. Fig. 5 shows the influence lines for the longitudinal strains of the three measurement stations and the ESFs of AB and BC under Loading Case 1.

Vehicle Model

In the numerical study, three typical highway trucks were adopted. Fig. 6 shows the axle configuration of the three trucks. Each truck was modeled by mass-spring-dashpot systems. As an example, the vehicle model for the five-axle truck is shown in Fig. 7. Detail properties of the three vehicles can be found in Harris et al. (2007), Shi and Cai (2009), Wang and Liu (2000), Zhang et al. (2006), and Zhou and Chen (2015). In the simulation, five vehicle speeds from 10 to 30 m/s with an increment of 5 m/s; four different RSCs including smooth, very good, good, and average; and three loading cases including both single vehicle cases and cases with multiple vehicle presence were considered to simulate different scenarios of truck passing. Table 1 summarizes the parameters considered in the numerical simulation.

Identification Results for Single-Vehicle Cases

For the single-vehicle cases, the truck either traveled along the centerline of the bridge or along the center of the left lane. Fig. 8 shows the typical longitudinal strain responses and the calculated ESFs under the passage of the 2-axle truck. Fig. 9 shows the ESFs of Girder 2 and the detected peaks and valleys under the passage of each truck at the speed of 20 m/s. For the purpose of demonstration, only the responses for the smooth and average RSCs while the truck traveled along the center of the roadway are presented. Fig. 9 shows that clear peaks and valleys are observed and that the number of peaks and valleys is the same as the number of vehicle axles, except for the case of the 5-axle truck in which only three peaks or valleys are found. For the 5-axle truck, the three rear axles are closely spaced, which resulted in only one identifiable peak and valley. It should be mentioned that the difficulty in identifying closely spaced axles has been reported by many researchers. Usually, the closely spaced axles, such as a tandem or tridem axle group, are identified as a single axle by most BWIM systems. In the present study, the three rear axles of the 5-axle truck are treated as a single axle with a weight of 218.7 kN. The equivalent AS between the second axle and the rear axle group is calculated as

$$\mathrm{AS}_2{}' = \sum_{i=3}^{5} \mathrm{AW}_i \left(\sum_{j=2}^{i-1} \mathrm{AS}_j \right) \Big/ \sum_{i=3}^{5} \mathrm{AW}_i \tag{12}$$

where AW_i = weight of the ith axle; and AS_j = spacing between the $(i-1)$th axle and the ith axle.

Using the proposed method, the vehicle speed and AS were calculated. For each RSC, five vehicle speeds were considered, and for each set of RSCs and each vehicle speed, 10 runs with 10 randomly generated road surface profiles were performed using the BVI simulation. Then, the RMS of the 10 results is calculated for the error analysis. Table 2 gives the RMSs of the relative errors (%) in the identification results.

Table 2 shows that (1) the proposed method can effectively identify the vehicle speed and AS. The RMSs of the identification errors are all within 5% for the vehicle speed and AS. (2) The identification errors of the three-axle truck are relatively larger than those of the other two trucks. This is because the weight proportion of the first axle to the gross vehicle weight (GVW) of the three-axle truck is low (only 11%), which causes the peaks and valleys corresponding to this axle susceptible to the dynamic effects in the strain response. Nevertheless, the identification accuracy is still acceptable. (3) For smooth RSCs and the 2-axle truck, the identification error increases gradually as the speed increases. However, the vehicle speed generally does not seem to have a significant impact on the identification accuracy. (4) RSC affects the identification accuracy because the rough surface tends to induce more vibrations and decrease the identification accuracy. Nevertheless, the identification results still show a satisfactory degree of accuracy under the average RSC.

The results obtained using the proposed ESF method in this study were also compared with those obtained using the virtual simply supported beam (VSSB) method proposed by He et al. (2017)

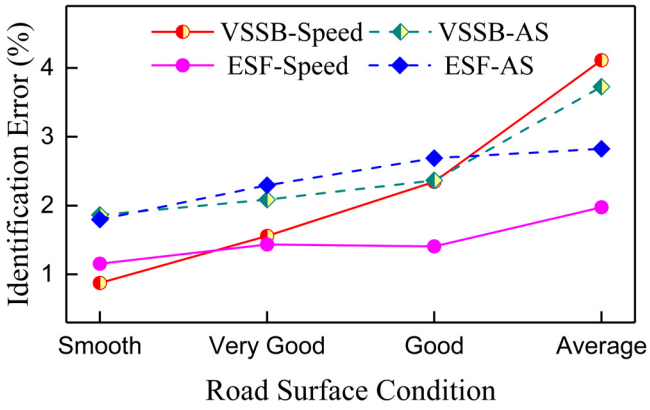

Fig. 10. RMS of relative error of identification results.

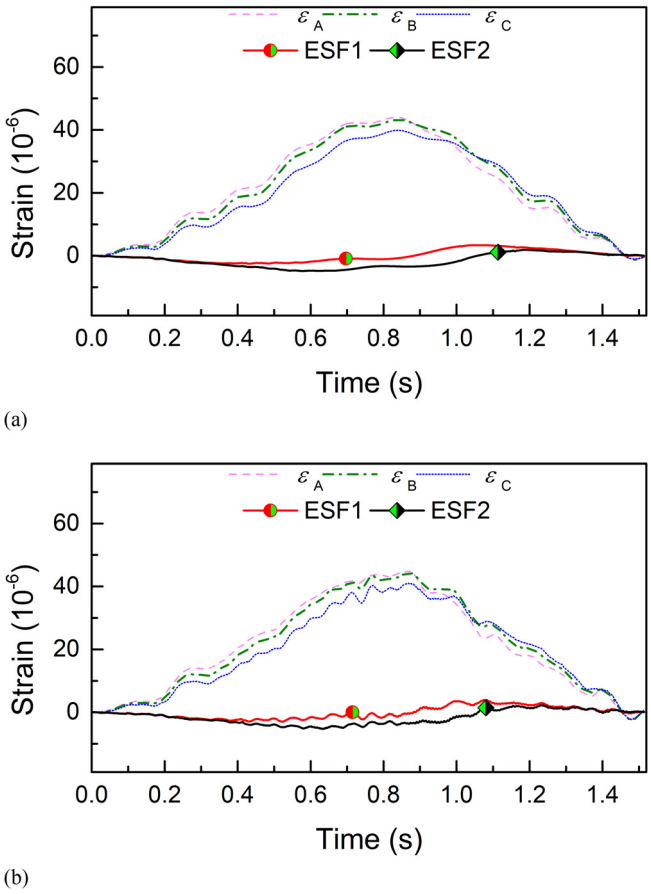

Fig. 11. Simulated bending strain and ESF of Girder 3 (Loading Case 2, 5-axle truck, $v = 20$ m/s): (a) smooth RSC; and (b) average RSC.

under the same cases. The RMS of relative error of the identified speed and ASs under all cases using both methods are plotted in Fig. 10. From Fig. 10, it was found that when the RSC is better than good, the two methods achieved similar identification accuracy. However, the proposed ESF method seems more reliable because the identification errors did not vary significantly under the different RSCs compared with the VSSB method.

In addition, the identification results for Loading Case 2 are very similar to those for Loading Case 1 when measurement stations are selected on Girder 2; thus, they are not presented here for the sake of brevity. Meanwhile, to investigate the effect of the transverse location of the measurement stations, three measurement stations with the same longitudinal location as those on Girder 2 were selected on Girder 3, and Fig. 11 shows the bending strain time histories and the ESFs for the 5-axle truck passing at a speed of 20 m/s under Loading Case 2. It can be seen that the ESFs of Girder 3 do not show clear peaks or valleys, making it infeasible to identify the vehicle axles. This is because when the vehicle was positioned in Lane 1, the shear forces induced on Girder 3 are so small that the peaks and valleys are not easily identifiable. This also indicates that two groups of measurement stations are required for each traffic lane to capture the information of all vehicles passing over the bridge. Also, the ESF signal under different traffic lanes can potentially be used to determine the traveling lane of the vehicle.

Table 3. Driving plans of two trucks in different lanes (Loading Case 3)

Driving plan	Description
1	Two trucks enter bridge at the same time at the same speed (from 10 to 30 m/s)
2	Two trucks travel at the same speed (from 10 to 30 m/s) with headway distance of either 5 m or 10 m
3	Two trucks enter bridge at the same time while the speed of the 2-axle truck was kept at 20 m/s, but the 3-axle truck's speed varies from10 to 30 m/s

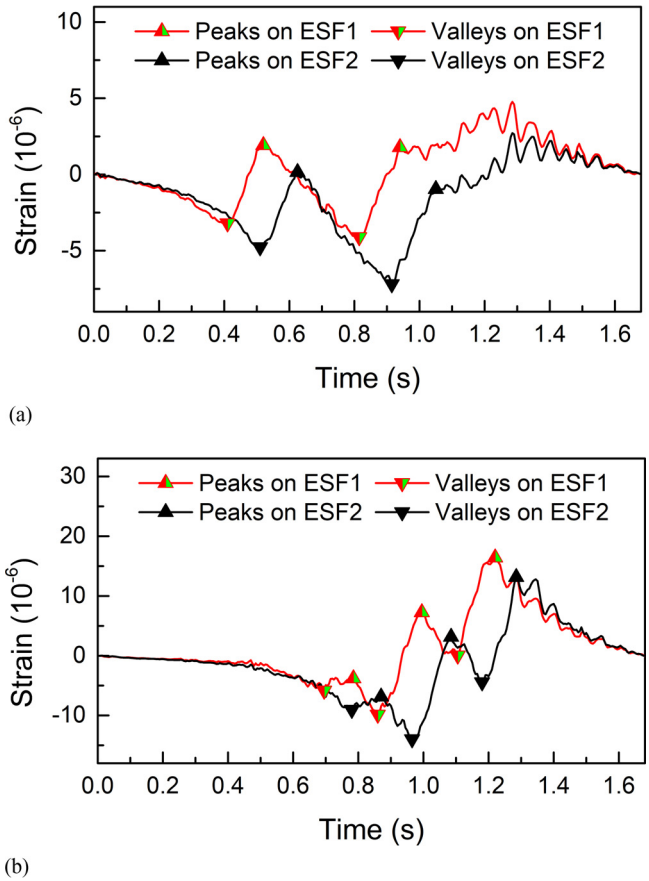

Fig. 12. Time histories of simulated bending strains and ESFs (average RSC, v = 20 m/s, head-to-head distance = 5 m): (a) Girder 2; and (b) Girder 3.

Identification Results for Cases with Multiple Truck Presence

In this study, a loading case with a 2-axle truck traveling in Lane 1 and a 3-axle truck traveling in Lane 2 were considered, as presented in Fig. 3(b). To represent real traffic, three driving plans were developed and summarized in Table 3.

Fig. 12 shows the time history of the simulated strain response and the ESFs for Girders 2 and 3 following the first driving plan. From Fig. 12, it can be seen that the peaks and valleys on the ESF time histories for both girders can still be clearly identified when the two trucks passed over the bridge simultaneously. For Girder 2, the ESF shows two groups of peaks and valleys corresponding to the 2-axle truck, whereas for Girder 3 the ESF shows three groups of peaks and valleys corresponding to the 3-axle truck. It should be noted that there were false peaks in Fig. 12(a) that occurred at the same time as the third peak on ESF2 in Fig. 12(b), and these false peaks should be excluded. The RMS of relative identification errors

Table 4. RMS of relative errors of identification results of two trucks traveling at the same speed

Head-to-head distance (m)	Speed (m/s)	RMS of relative errors (%)				
		2-axle truck		3-axle truck		
		v	AS	v	AS_1	AS_2
0	10	0.90	1.54	1.07	1.90	1.86
	15	1.05	0.83	1.44	0.92	1.83
	20	1.03	1.11	1.15	1.71	2.04
	25	1.25	1.56	1.94	0.95	1.30
	30	0.92	0.95	1.55	1.81	1.56
5	10	1.50	1.39	1.02	1.88	1.29
	15	1.51	1.80	1.56	2.53	1.68
	20	2.26	2.25	1.14	2.07	2.63
	25	1.03	2.23	2.21	2.29	2.45
	30	2.60	1.85	1.53	1.56	1.77
10	10	0.87	1.04	0.76	2.40	2.52
	15	0.86	2.05	1.44	1.29	1.37
	20	1.13	0.76	2.03	2.77	1.53
	25	1.33	1.77	1.96	2.85	1.94
	30	2.47	1.71	1.89	1.49	2.46

Table 5. RMS of relative errors of identification results of two trucks traveling at different speeds

Speed (m/s)		RMS of relative errors (%)				
		2-axle truck		3-axle truck		
Truck 1	Truck 2	v	AS	v	AS_1	AS_2
20	10	2.35	1.71	0.66	2.04	1.60
	15	1.45	1.89	1.51	1.79	1.62
	20	1.03	1.11	1.15	1.71	2.04
	25	1.14	2.09	1.57	2.17	1.91
	30	1.66	1.68	1.43	1.53	2.03

Note: AS = axle spacing.

(%) for Driving Plans 1 and 2 are presented in Table 4, and the RMS of relative identification errors (%) for Driving Plan 3 are summarized in Table 5. Good accuracy was achieved in the identified vehicle speed and axles for both trucks, suggesting that the proposed method is able to deal with cases with multiple vehicle presence.

Experimental Validation

Experiment Setup

To validate the effectiveness of the proposed method, laboratory experiments were conducted using a BVI test platform, as shown in Fig. 13. The BVI test platform consists of an accelerating ramp, a bridge model, and a deceleration zone.

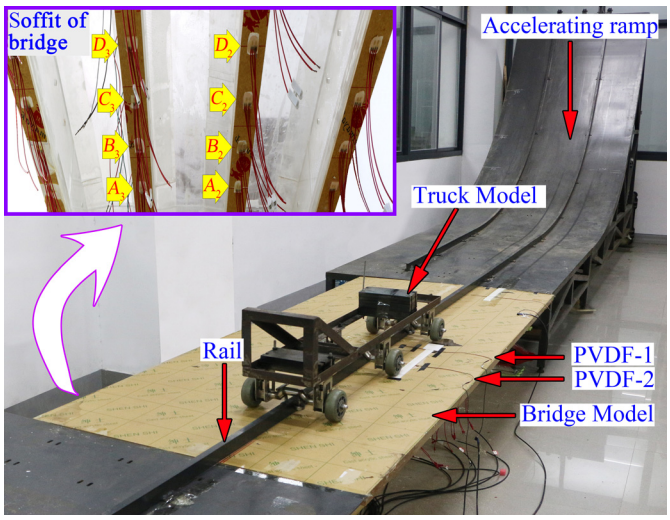

Fig. 13. BVI test platform. PVDF = polyvinylidene fluoride.

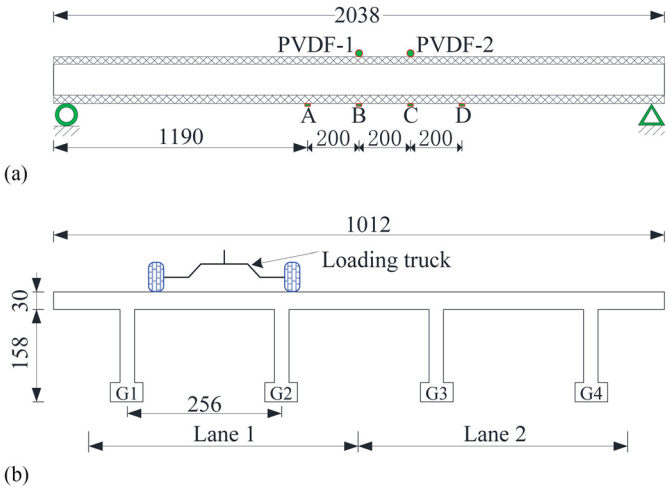

Fig. 14. Scaled bridge model: (a) longitudinal profile and location of sensors; and (b) cross section (unit: millimeters).

The laboratory bridge model was fabricated based on the bridge model adopted in the simulation study with a scale ratio of 1 to 0.119. The model is fabricated using polymethyl methacrylate (PMMA) material, which has an elastic modulus of 2,795 MPa and a density of 1,181.6 kg/m^3. More information of the bridge model can be found in He et al. (2017). Fig. 14(a) shows the cross section of the scaled bridge model and the truck loading position. Four foil strain gauges were attached underneath Girder G2 and two polyvinylidene fluoride (PVDF) cables were mounted on the deck surface to measure the vehicle speed, as shown in Fig. 14(b). The strains measured at Gauges A, B, and C were used to calculate the ESFs.

The test truck model shown in Fig. 13 was built based on a three-axle truck with a GVW of 248 kN. The AS of the test truck model can be adjusted to reproduce different axle configurations. The axle configuration of the scaled truck model adopted in this study and the corresponding full-scale prototype truck model (based on the similar principle) are given in Table 6. During the test, the vehicle was first hauled to a certain height on the accelerating ramp using a rope. Then, the rope was released and the vehicle gained speed under the effect of gravity and passed over the bridge model. Because of safety concerns and the height limitation of the ramp, the maximum speed of the truck model was limited to 5 m/s. In addition, it should be noted that the experiment was not conducted under a perfectly smooth road surface profile. During the fabrication of the models, a gap between the ramp and the model bridge is inevitable, which could serve as a source of excitation when the vehicle enters the bridge. Therefore, the dynamic effect still exists during the experiment and could potentially cause identification errors.

Result Analysis

In the experimental study, three different loading positions were considered to study the effect of the vehicle's lateral position on the identification accuracy. The vehicle either travels along the left edge of Lane 1, or the center of Lane 1, or the right edge of Lane 1. The vehicle position can be changed by adjusting the position of the rail track. It should be mentioned that the vehicle was only

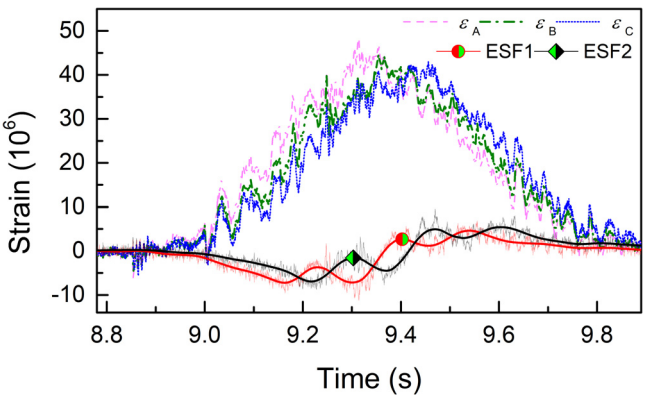

Fig. 15. Typical measured strains and ESFs.

Table 6. Axle weight and spacing of test truck model

Truck model	AS_1 (m)	AS_2 (m)	AW_1 (N)	AW_2 (N)	AW_3 (N)
Test model (scaled)	0.454	0.472	88.180	136.926	59.486
Prototype (full-scale)	3.820	3.970	76.83×10^3	119.36×10^3	51.84×10^3

Note: AS = axle spacing; AW = axle weights.

positioned in Lane 1 due to the symmetry of the bridge about its centerline. Moreover, the effect of the vehicle speed was also investigated. In the experimental study, the vehicle speed was varied from 1 to 5 m/s by adjusting the height of the truck model on the acceleration ramp. The minimum and maximum vehicle speeds correspond to 10.4 and 52 km/h for the corresponding full-scale truck, respectively.

Fig. 15 shows the strains measured from Girder 2 and the derived ESFs under the case with the truck traveling along the left edge of Lane 1 at a speed of 3.05 m/s. To reduce the effects of bridge dynamic vibration and measurement noise, a moving average filter, which is provided by the MATLAB platform, was used to smooth the time histories of the ESF through local regression by adopting weighted linear least squares and a second-order polynomial model. During the smoothing, each data point of the filtered signal was calculated using a span of 5% of the total number of data points. From Fig. 15, it can be seen that the peaks and valleys on the filtered ESF time histories are more distinctive than those on the original ESF time histories.

Fig. 16 shows the derived ESF time histories of a test series in which the vehicle passed over the bridge along different lateral positions at a speed of approximately 3 m/s. It should be noted that in

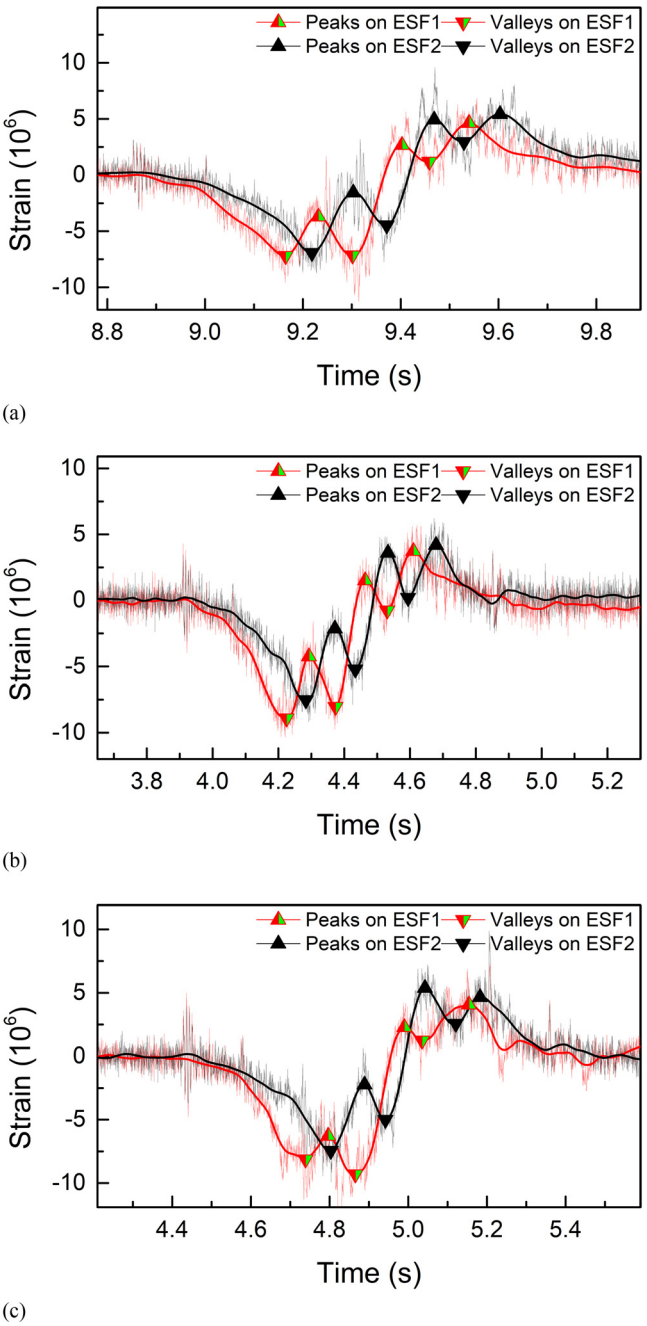

Fig. 16. Time histories of the ESFs for a test series with the vehicle traveling along (a) the left edge of Lane 1 at 3.05 m/s (31.87 km/h at full-scale); (b) the center of Lane 1 at 3.02 m/s (31.46 km/h at full-scale); and (c) the right edge of Lane 1 at 3.00 m/s (31.31 km/h at full-scale).

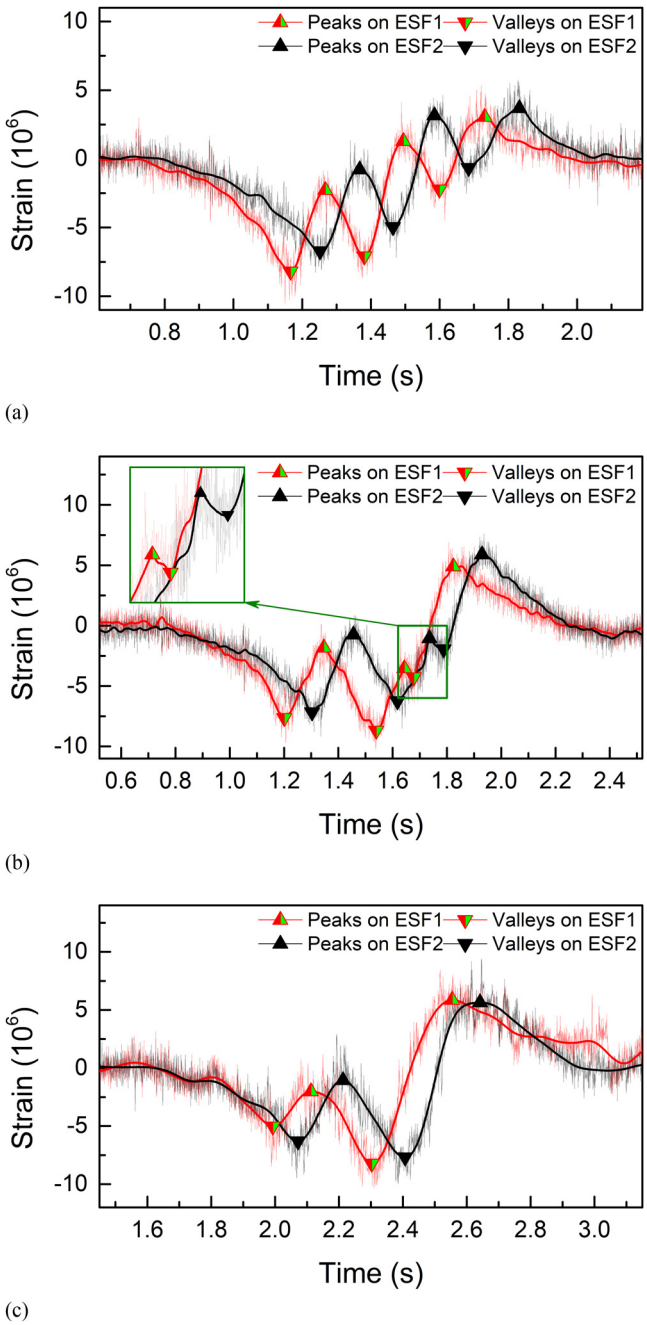

Fig. 17. Time histories of the ESF with the three truck models traveling along the right edge of Lane 1: (a) Truck Model 1; (b) Truck Model 2; and (c) Truck Model 3.

Figs. 16 and 17 the relatively smooth signals correspond to the filtered responses using the moving average filter, whereas the oscillating signals correspond to the unfiltered responses. Fig. 16 shows that three groups of clear peaks and valleys were observed corresponding to the three axles passing the ESF segments regardless of the lateral position of the vehicle, which indicates that the change of vehicle's lateral position within the traffic lane does not affect the identification accuracy of the proposed ESF method. In this case, only two girders, i.e., G2 and G3, need to be instrumented to identify all vehicles traveling in either traffic lane of this bridge.

Table 7 lists the relative identification errors (%) by the proposed ESF method. For comparison, also included in Table 7 are the relative identification errors obtained using PVDF cables and the VSSB method (He et al. 2017). The vehicle speeds v^P obtained using the PVDF cables were considered as the true values to evaluate the accuracy of the predicted speeds by the VSSB method and the proposed ESF method. Table 7 shows that acceptable identification accuracy of the vehicle speed and AS is achieved using the proposed ESF method because the errors of most cases are within 4% regardless of the vehicle's speed and lateral position. Furthermore, the identification accuracy of AS obtained using the ESF method is within the same range as those obtained using the PVDF method, indicating that the proposed ESF method has the potential to achieve the same level of accuracy as the pavement-based axle detection methods, which are typically considered to be the most accurate methods of axle detection in BWIM systems.

Finally, to study the effect of AS on the accuracy and the effectiveness of the proposed ESF method, three different axle configurations of the test truck were considered with details provided in Table 8. Figs. 17(a–c) show the time histories of the ESFs when the three truck models passed over the bridge at a speed of approximately 2 m/s, respectively. Fig. 17(a) shows that three groups of distinctive peaks and valleys can be found on each ESF time history when the spacing of the two rear axles is 472 mm. Nevertheless, when the AS of the two rear axles decreases to 312 mm (about 1.5 times the distance between two adjacent strain gauges), the second peak corresponding to the second axle passing over Sensor B and the third valley corresponding to the third axle passing over Sensor A becomes very close, making it more difficult to identify the two axles, as seen in Fig. 17(b). When the rear axle spacing was further reduced to almost the sensor spacing, as was the case of Truck 3, the second peak and the third valley may have merged; thus, the second and third axles of the truck model cannot be identified individually, as can be seen from Fig. 17(c). In this case, the two rear axles will be treated as an axle group, and the equivalent static AS between the first axle and the rear axle group is calculated as

$$AS = AS_1 + \frac{AW_3}{AW_2 + AW_3} \times AS_2 \tag{13}$$

The relative identification errors using the three truck models are listed in Table 9. Table 9 shows that the ESF method can accurately identify the vehicle speed for different axle configurations. However, the identification accuracy of AS decreases as the AS becomes smaller. As a general rule of thumb, it is suggested that the minimum AS is at least 1.5 times the distance between the two sensors within a measurement group.

Summary and Conclusions

In this study, a novel axle detection strategy, i.e., the ESF method, was proposed to identify the speed and the AS of moving vehicles on bridges. The proposed ESF method uses the global bending strains of bridges to achieve axle detection and thus can be used for the NOR BWIM systems. Numerical and experimental studies were

Table 8. Different AS schemes tested

Truck model number	AS_1 (m)	AS_2 (m)
1	0.454 (3.82)	0.472 (3.97)
2	0.612 (5.14)	0.312 (2.62)
3	0.709 (5.96)	0.208 (1.74)

Note: Values in parentheses are the corresponding values for the corresponding full-scale truck model based on a similar principle.

Table 7. Relative errors of identification results

			Relative errors (%)							
			PVDF		VSSB			ESF		
Vehicle lateral position	v^P (m/s)	$v^{\text{full-scale}}$ (km/h)	AS_1	AS_2	v	AS_1	AS_2	v	AS_1	AS_2
Left edge of Lane 1	1.00	10.45	−2.65	1.49	−0.66	−1.92	−0.39	0.86	−0.25	1.91
	2.07	21.59	−1.45	−0.83	2.65	1.63	2.37	2.29	3.20	1.56
	3.05	31.87	0.88	−0.86	−0.51	3.55	−3.13	−0.00	2.99	−3.45
	4.04	42.17	−0.99	−0.06	1.71	0.93	2.30	2.15	2.95	−0.43
	5.02	52.40	−0.19	1.32	−5.16	−3.24	−4.16	−1.75	4.72	1.12
Center of Lane 1	0.97	10.11	−2.72	1.01	0.81	−1.23	1.62	0.08	0.53	0.76
	2.04	21.26	−0.82	0.46	−0.17	−0.88	−0.14	1.29	3.30	3.18
	3.02	31.46	0.12	0.45	−0.50	0.11	0.90	1.08	4.13	−0.89
	3.97	41.47	−2.41	−4.45	1.00	−7.84	0.33	3.69	1.64	−1.58
	5.13	53.52	−0.60	0.23	−3.31	−2.25	−2.03	0.86	3.68	−0.41
Right edge of Lane 1	1.03	10.74	−0.26	3.08	−2.91	−4.21	1.50	−1.75	2.65	3.45
	2.07	21.59	0.60	2.68	−4.13	−5.20	−1.67	−2.93	2.35	0.21
	3.00	31.31	0.11	−1.64	0.25	3.01	−3.94	−0.06	3.27	2.82
	4.07	42.45	1.69	3.20	1.03	4.32	4.48	−4.76	3.79	1.57
	5.06	52.84	3.72	6.20	−0.42	0.23	10.56	−3.27	4.38	5.20
RMS	—	—	1.68	2.51	2.27	3.38	3.63	2.25	3.18	2.35

Note: AS = axle spacing; ESF = equivalent shear force; PVDF = polyvinylidene fluoride; and VSSB = virtual simply supported beam. $v^{\text{full-scale}}$ = the vehicle speed of the corresponding full-scale truck model based on the similar principle; and v^P = vehicle speed identified using PVDF.

Table 9. Relative errors of identification results for truck models with different ASs

			Relative errors (%)				
			PVDF		ESF		
Truck model	v^P (m/s)	$v^{\text{full-scale}}$ (km/h)	AS_1	AS_2	v	AS_1	AS_2
1	2.07	21.59	−1.45	−0.83	2.65	3.27	1.75
2	1.92	20.00	−4.00	0.30	0.32	−0.94	6.86
3	1.99	22.40	1.55	0.15	0.18	1.93[a]	

Note: AS = axle spacing; ESF = equivalent shear force; PVDF = polyvinylidene fluoride.

[a]Equivalent AS between the front axle and the rear axle group [the true value is calculated to be 0.787 m using Eq. (13)].

conducted to demonstrate the performance of the proposed ESF method. The identification results showed that the proposed ESF method can provide accurate and reliable axle detection for the NOR BWIM systems. The effects of measurement location, vehicle speed, the vehicle's lateral position, RSC, multiple vehicle presence, and AS on the identification accuracy were investigated.

The following conclusions can be drawn based on the results from this study: (1) to identify vehicles traveling in a particular lane, strain sensors need to be installed underneath that lane; (2) the vehicle's speed and lateral position do not affect the identification accuracy; (3) the identification accuracy decreases as the RSC worsens, nevertheless, the identification accuracy is still acceptable under the average RSC; and (4) when the AS approaches the sensor spacing, the identification of individual axles becomes more difficult. To be able to identify each individual axle in a group of closely spaced axles, the AS should be at least 1.5 times the sensor spacing; otherwise, the closely spaced axles may be identified as a single axle. In addition, based on the numerical study, it is found that the ESF method is able to identify vehicle speed and AS under the cases with multiple vehicle presence.

Compared with traditional NOR axle detection methods, such as the FAD methods, the ESF method uses the global bending response of bridges; thus, it is applicable to most bridges whose dominant internal force is the bending moment under vehicle loading. Furthermore, the ESF is not susceptible to the lateral position of the vehicles and can be used to identify multiple vehicle presence. These advantages make the ESF method a reliable strategy of axle detection for commercial NOR BWIM systems. Future studies will focus on developing algorithms for automatic identification of vehicle axles using the ESF method and testing the performance of the ESF method in full-scale experiments.

Acknowledgments

The authors acknowledge the financial support provided by the National Natural Science Foundation of China (Grants 51478176 and 51778222) and the Key Research Project of Hunan Province (Grant 2017SK2224).

References

Bao, T., S. Babanajad, T. Taylor, and F. Ansari. 2016. "Generalized method and monitoring technique for shear-strain-based bridge weigh-in-motion." *J. Bridge. Eng.* 21 (1): 04015029. https://doi.org/10.1061/(ASCE)BE.1943-5592.0000782.

Cai, C. S., X. Shi, M. S. Araujo, and S. Chen. 2007. "Influence of approach span conditions on vehicle-induced dynamic response of slab-on-girder bridges: Field and numerical simulations." In *Proc., Transportation Research Board 86th Annual Meeting*. Washington, DC: Transportation Research Board.

Chatterjee, P., E. J. O'Brien, Y. Li, and A. González. 2006. "Wavelet domain analysis for identification of vehicle axles from bridge measurements." *Comput. Struct.* 84 (28): 1792–1801. https://doi.org/10.1016/j.compstruc.2006.04.013.

Deng, L., and C. S. Cai. 2010a. "Development of dynamic impact factor for performance evaluation of existing multi-girder concrete bridges." *Eng. Struct.* 32 (1): 21–31. https://doi.org/10.1016/j.engstruct.2009.08.013.

Deng, L., and C. S. Cai. 2010b. "Identification of dynamic vehicular axle loads: Theory and simulations." *J. Vib. Control* 16 (14): 2167–2194. https://doi.org/10.1177/1077546309351221.

Deng, L., and C. S. Cai. 2011. "Identification of dynamic vehicular axle loads: Demonstration by a field study." *J. Vib. Control* 17 (2): 183–195. https://doi.org/10.1177/1077546309351222.

Dodds, C. J., and J. D. Robson. 1973. "The description of road surface roughness." *J. Sound Vib.* 31 (2): 175–183. https://doi.org/10.1016/S0022-460X(73)80373-6.

Dunne, D., E. J. O'Brien, B. Basu, and A. Gonzalez. 2005. "Bridge WIM systems with Nothing on the Road (NOR)." In *Proc., 4th Int. Conf. on Weigh-in-Motion*. Taipei, Taiwan: International Society for Weigh-in-Motion.

Harris, N. K., E. J. O'Brien, and A. González. 2007. "Reduction of bridge dynamic amplification through adjustment of vehicle suspension damping." *J. Sound. Vib.* 302 (3): 471–485. https://doi.org/10.1016/j.jsv.2006.11.020.

He, W., L. Deng, H. Shi, C. Cai, and Y. Yu. 2017. "Novel virtual simply supported beam method for detecting the speed and axles of moving vehicles on bridges." *J. Bridge Eng.* 22 (4): 04016141. https://doi.org/10.1061/(ASCE)BE.1943-5592.0001019.

Ieng, S. S., A. Zermane, F. Schmidt, and B. Jacob. 2012. "Analysis of B-WIM signals acquired in Millau orthotropic viaduct using statistical classification." In *Proc., Int. Conf. on Weigh-in-Motion: ICWIM 6*, 43–52. Hoboken, NJ: Wiley.

ISO. 1995. *Mechanical vibration–road surface profiles–reporting of measured data*. ISO 8608. Geneva: ISO.

Jacob, B., and E. J. O'Brien. 1998. "European specification on weigh-in-motion of road vehicles (COST323)." In *Proc., 2nd European Conf. on Weigh-in-Motion of Road Vehicles*. Luxembourg: Office for Official Publications of the European Commission.

Jacob, B., and E. J. O'Brien. 2005. "Weigh-in-motion: Recent developments in Europe." In *Proc., 4th Int. Conf. on Weigh-in-Motion*. Dubendorf, Switzerland: International Society for Weigh-in-Motion.

Kalhori, H., M. M. Alamdari, X. Zhu, B. Samali, and S. Mustapha. 2017. "Non-intrusive schemes for speed and axle identification in bridge-weigh-in-motion systems." *Meas. Sci. Technol.* 28 (2): 025102. https://doi.org/10.1088/1361-6501/aa52ec.

Kalin, J., A. Žnidarič, and I. Lavrič. 2006. "Practical implementation of nothing-on-the-road bridge weigh-in-motion system." In *Proc., 9th Int. Symp. on Heavy Vehicle Weights and Dimensions*. State College, Pennsylvania: Pennsylvania State University.

Laboratoire Central des Ponts et Chaussées. 2001. *Weighing-in-motion of axles and vehicles for Europe (WAVE)*. Rep. of work package 1.2. Paris: Laboratoire Central des Ponts et Chaussées.

Lechner, B., M. Lieschnegg, O. Mariani, M. Pircher, and A. Fuchs. 2010. "A wavelet-based bridge weigh-in-motion system." *Int. J. Smart Sens. Intell. Syst.* 3 (4): 573–591. https://doi.org/10.21307/ijssis-2017-409.

Lydon, M., D. Robinson, S. E. Taylor, G. Amato, E. J. O'Brien, and N. Uddin. 2017. "Improved axle detection for bridge weigh-in-motion systems using fiber optic sensors." *J. Civ. Struct. Health Monit.* 7 (3): 325–332. https://doi.org/10.1007/s13349-017-0229-4.

Lydon, M., S. E. Taylor, D. Robinson, A. Mufti, and E. J. O'Brien. 2016. "Recent developments in bridge weigh in motion (B-WIM)." *J. Civ. Struct. Health Monit.* 6 (1): 69–81. https://doi.org/10.1007/s13349-015-0119-6.

Moses, F. 1979. "Weigh-in-motion system using instrumented bridges." *Transp. Eng. J.* 105 (3): 233–249.

O'Brien, E. J., D. Hajializadeh, N. Uddin, D. Robinson, and R. Opitz. 2012. "Strategies for axle detection in bridge weigh-in-motion systems." In *Proc., Int. Conf. on Weigh-in-Motion: ICWIM 6.* Hoboken, NJ: Wiley.

O'Brien, E. J., C. W. Rowley, A. Gonzalez, and M. F. Green. 2009. "A regularised solution to the bridge weigh-in-motion equations." *Int. J. Heavy Veh. Syst.* 16 (3): 310–327. https://doi.org/10.1504/IJHVS.2009.027135.

Ojio, T., C. Carey, E. O'Brien, C. Doherty, and S. Taylor. 2016. "Contactless bridge weigh-in-motion." *J. Bridge Eng.* 21 (7): 04016032. https://doi.org/10.1061/(ASCE)BE.1943-5592.0000776.

Peters, R. 1984. "AXWAY-a system to obtain vehicle axle weights." *Aust. Road Res.* 12 (2): 10–18.

Shi, X., and C. Cai. 2009. "Simulation of dynamic effects of vehicles on pavement using a 3D interaction model." *J. Transp. Eng.* 135 (10): 736–744. https://doi.org/10.1061/(ASCE)TE.1943-5436.0000045.

Wall, C. J., R. E. Christenson, A. M. H. Mcdonnell, and A. Jamalipour. 2009. *A non-intrusive bridge weigh-in-motion system for a single span steel girder bridge using only strain measurements.* Rep. No. CT-2251-3-09-5, 9–10. Rocky Hill, CT: Connecticut DOT.

Wang, T. L., and C. H. Liu. 2000. *Influence of heavy trucks on highway bridges.* Rep. No. FL/DOT/RMC/6672-379. Tallahassee, FL: Florida DOT.

Yu, Y., C. S. Cai, and L. Deng. 2016. "State-of-the-art review on bridge weigh-in-motion technology." *Adv. Struct. Eng.* 19 (9): 1514–1530. https://doi.org/10.1177/1369433216655922.

Yu, Y., C. S. Cai, and L. Deng. 2017a. "Nothing-on-road bridge weigh-in-motion considering the transverse position of the vehicle." *Struct. Infrastruct. Eng.* 1–15. https://doi.org/10.1080/15732479.2017.1401095.

Yu, Y., C. S. Cai, and L. Deng. 2017b. "Vehicle axle identification using wavelet analysis of bridge global responses." *J. Vib. Control* 23 (17): 2830–2840. https://doi.org/10.1177/1077546315623147.

Zhang, Y., C. Cai, X. Shi, and C. Wang. 2006. "Vehicle-induced dynamic performance of FRP versus concrete slab bridge." *J. Bridge. Eng.* 11 (4): 410–419. https://doi.org/10.1061/(ASCE)1084-0702(2006)11:4(410).

Zhao, H., N. Uddin, X. Shao, P. Zhu, and C. Tan. 2014. "Field-calibrated influence lines for improved axle weight identification with a bridge weigh-in-motion system." *Struct. Infrastruct. Eng.* 11 (6): 721–743. https://doi.org/10.1080/15732479.2014.904383.

Zhou, Y., and S. Chen. 2015. "Fully coupled driving safety analysis of moving traffic on long-span bridges subjected to crosswind." *J. Wind. Eng. Ind. Aerodyn.* 143 (Aug): 1–18. https://doi.org/10.1016/j.jweia.2015.04.015.

Žnidarič, A., G. Turk, and E. Zupan. 2015. "Determination of strain correction factors for bridge weigh-in-motion systems." *Eng. Struct.* 102 (Nov): 387–394. https://doi.org/10.1016/j.engstruct.2015.08.026.

Zolghadri, N., M. Halling, N. Johnson, and P. Barr. 2016. "Field verification of simplified bridge weigh-in-motion techniques." *J. Bridge. Eng.* 21 (10): 04016063. https://doi.org/10.1061/(ASCE)BE.1943-5592.0000930.